Potential Vorticity Diagnosis of a Tropopause Polar Cyclone

Steven M. Cavallo* & Gregory J. Hakim

University of Washington, Seattle, WA

*Corresponding author address: Steven Cavallo, Department of Atmospheric Sciences, Box 351640, University of Washington, Seattle, WA 98195-1640.
E-mail: scavallo@atmos.washington.edu

Abstract

Long-lived coherent vortices based on the tropopause are often found over polar regions, where potential vorticity gradients are weaker than in midlatitudes. Although these vortices are a commonly observed feature of the Arctic, and can have lifetimes longer than one month, little is known about the mechanisms that control their evolution. This paper examines mechanisms of intensity change for a cyclonic tropopause polar vortex (TPV) using an Ertel potential vorticity (EPV) diagnostic framework.

Results from a climatology of intensifying cyclonic TPVs suggest that the essential dynamics are local to the vortex, rather than a consequence of larger scale processes. This fact motivates a case study using a numerical model to investigate the role of diabatic mechanisms in the growth and decay of a particular cyclonic vortex. A component-wise breakdown of EPV reveals that cloud-top radiational cooling is the primary diabatic mechanism that intensifies the TPV during the growth phase. Increasing amounts of moisture become entrained into the vortex core at later times near Hudson Bay, allowing the destruction of potential vorticity near the tropopause due to latent heating to become comparable to the radiational tendency to create potential vorticity.

1. Introduction

Tropopause vortices are extratropical, cold-core cyclones or anticyclones, defined by closed material contours. On the dynamic tropopause, taken to be a potential vorticity (PV) surface, cyclones are characterized by relatively high pressure and low potential temperature while anticyclones are characterized by relatively low pressure and high potential temperature. Although these vortices are present in mid-latitudes, they occur frequently over the polar regions, where PV gradients are weaker than in midlatitudes and there is greater isolation from the jet stream (Hakim and Canavan 2005). Horizontal length scales of these tropopause polar vortices (TPVs) are most often less than 1000 km in radius, and their lifespan can extend beyond one month (Hakim and Canavan 2005). Despite their ubiquity and longevity, little is known about the mechanisms that control their evolution. This study focuses on mechanisms affecting cyclonic vortex intensity, and specifically examines the life cycle of an observed event using a numerical model and PV diagnostic framework.

In the context of PV, vortex amplitude on the dynamic tropopause can be defined by the range of closed contours of potential temperature.[1] Therefore, changes in vortex strength require non-conservative diabatic or frictional processes (e.g. Pedlosky 1998, section 2.5). This PV perspective has been applied extensively to studies of warm-core cyclones, where significant latent heating has been shown to affect vortex intensity (e.g. Shapiro and Willoughby 1982; Schubert and Hack 1983; Nolan and Grasso 2003). In these cases, latent heating produces low-level PV, which intensifies the vortex where it is strongest.

Several studies have addressed the effect of diabatic processes on the PV distribution

[1] Assuming adiabatic and inviscid flow, PV and potential temperature are both conserved following the fluid motion. Thus the existence of closed PV contours on potential temperature surfaces implies the existence of closed contours of potential temperature on PV surfaces.

near extratropical cyclones. For example, Davis and Emanuel use a piecewise PV inversion methodology in a case study quantifying the development of a low-level PV anomaly produced by latent heating. They found that this low-level PV anomaly subsequently contributed to the reduction of downstream tropopause-level PV. Using a similar technique in a numerical modelling study Stoelinga (1996) showed that latent heating destroyed upper-level PV downstream and above the latent heating source in the direction of the absolute vorticity vector, consistent with theoretical expectations.

Fewer studies have examined non-conservative PV processes on the dynamics of isolated cold-core extratropical vortices. Since cold-core vortices strengthen upward in the troposphere, low-level latent heating typically destroys upper-level PV, leading to a weaker vortex (e.g. Hoskins et al. 1985, section 7). For example, Wirth (1995) performed an idealized study of an axisymmetric tropopause cyclone and found that a latent heat source located in the cyclone core acted to weaken the vortex considerably. Adding an idealized thin layer of modest cooling to simulate the effect of cloud-top radiational cooling had little affect on the cyclone evolution. However, increasing the magnitude of the cloud-top radiational cooling strengthened the vortex, suggesting that radiation may play a role in cyclonic vortex intensity change, depending on the exact magnitude and location of the cloud-top radiational cooling relative to the tropopause (Wirth 1995). Idealized radiational cooling in isolation was shown in a subsequent idealized study of an axisymmetric vortex to create upper-level PV and lower the tropopause (Zierl and Wirth 1997). The authors are not aware of studies that examine tropopause vortex intensity changes due to the interactive effects of latent heating and cloud-top radiational cooling.

Regarding observations of TPVs, Hakim and Canavan (2005) performed an objective census and found an average of 15 cyclonic vortices per month, with a frequency maximum over

the Canadian Arctic. Here we extend these results by examining the vortex census results of Hakim and Canavan (2005) to identify regions of TPV genesis, growth, and decay. A numerical simulation of a particular case is then analyzed from a PV framework with the goal of investigating how diabatic processes affect vortex strength.

This paper is organized as follows. Section 2 provides a brief climatology of cyclonic TPV genesis and intensity change, the results of which suggest that the essential dynamics are local to the vortex rather than dependent on large-scale patterns. This finding motivates the use of PV diagnostics on a numerical simulation of a particular case over the Canadian Arctic. The theory and methodology for the PV diagnostics are described in Section 3, and an overview of the case study is provided in Section 4. A description of the numerical model and model simulation results from the case study, including a PV budget, are provided in Section 5. A concluding summary is given in Section 6.

2. Tropopause polar vortex climatology of intensification

Vortices are spatially localized structures characterized by trapped fluid particles, unlike waves, which may propagate energy. Vortices are identified here by the presence of closed contours of potential temperature on the dynamic tropopause, defined by a PV surface. Adiabatic conditions imply that fluid parcels located within closed contours act as tracers of the vortex. A change in the range of closed PV contours provide one objective measure of vortex intensity change, which we employ implicitly through the range of closed potential temperature contours on the PV surface representing the tropopause.

Regions of cyclonic TPV intensity change are determined from 2.5° NCEP/NCAR reanalysis data every six hours during 1948-1999 (Kalnay and collaborators 1996). Tropopause vortices

are identified as in Hakim and Canavan (2005) by objectively tracking TPVs on the 1.5 PVU (1 PVU is 1×10^{-6} K kg^{-1} s^{-1} m^2) EPV surface. Cyclonic vortex amplitude, defined as the difference between the local minimum in potential temperature (which we call the core value) and the last closed contour, is used to determine the strength of the vortices relative to their surroundings. TPVs are defined as in Hakim and Canavan (2005) to include only those vortices that spend at least 60% of their lifetimes north of 65°N and have a total lifetime of at least two days. To filter out spurious intensity changes, we discard any event for which there is a tropopause potential temperature amplitude change of at least 10 K followed by an amplitude change of at least 75% of the opposite sign within the following two time steps (12 hours); this eliminates 1.97% of the vortices. Vortex genesis is defined to occur by the identification of a local minimum in tropopause potential temperature that is colder than all other locations within a 650 km radius. Vortex lysis is defined to occur when a local minimum in tropopause potential temperature can no longer be identified with an existing vortex track. Growth (decay) refers to the greatest increase (decrease) in amplitude during a twenty-four hour period over the vortex lifetime.

Results show that TPV genesis occurs most frequently in the Canadian archipelago and northern Baffin Bay, with less dense areas along the northern Siberian coast (Fig. 1a). In general, cyclolysis densities are greatest just downstream of the maximum tropopause cyclogenesis regions, with the greatest density near the northwestern coast of Greenland and along the coast of northern Siberia near Severnaya Zemlya (Fig. 1b). Cyclone growth occurs most often near northern Baffin Island, with a secondary maximum over central Greenland, and smaller maxima along the northern coast of Siberia (Fig. 1c). Cyclone decay occurs most frequently along the northern shore of Baffin Island, with a secondary maximum over eastern

Greenland (Fig. 1d). The close proximity of the main TPV cyclogenesis and cyclolysis regions suggests that vortices form and spend most their lifetime in the same region. A compositing analysis revealed no significant relationship between large-scale patterns and cyclonic TPV intensity changes (not shown), suggesting that local factors are more important than large-scale circulation anomalies. These findings motivate a case study investigation of a TPV in order to examine vortex-scale processes from a PV framework.

3. PV diagnostics

a. Theory and methodology

Vortex intensity changes can be quantified using the Ertel PV tendency equation (e.g. Pedlosky 1998):

$$\frac{D\Pi}{Dt} = \frac{D}{Dt}\left(\frac{1}{\rho}\vec{\omega_a}\cdot\nabla\theta\right) = \frac{\vec{\omega_a}}{\rho}\cdot\nabla\frac{D\theta}{Dt} + \frac{\nabla\theta}{\rho}\cdot\left(\nabla\times\frac{\vec{F}}{\rho}\right). \tag{1}$$

Here, $\frac{D}{Dt} = \frac{\partial}{\partial t} + u\frac{\partial}{\partial x} + v\frac{\partial}{\partial y} + w\frac{\partial}{\partial z}$ is the time rate of change following the fluid, $\nabla = \left(\frac{\partial}{\partial x}, \frac{\partial}{\partial y}, \frac{\partial}{\partial z}\right)$ is the gradient operator, ρ is the fluid density, $\vec{U} = (u, v, w)$ is the three-dimensional wind vector, and $\vec{F}$ is the frictional force vector on momentum. The three-dimensional absolute vorticity vector is given by $\omega_a = \vec{\omega} + 2\vec{\Omega} = \nabla\times\vec{U} + 2\vec{\Omega}$, where $\vec{\Omega}$ is Earth's rotational vector, and $\Pi = \frac{1}{\rho}\vec{\omega_a}\cdot\nabla\theta$ is the Ertel PV (EPV). Potential temperature is given by $\theta = T\left(\frac{p_o}{p}\right)^{R/c_p}$, where T is temperature, p is pressure, $p_o = 10^5$ Pa is a standard constant, R = 287 J K^{-1} kg^{-1} is the dry air gas constant, and c_p = 1004 J K^{-1} kg^{-1} is the specific heat capacity of dry air at constant pressure. Given the PV-based definition of vortex amplitude adopted here, (1) implies that vortex intensity changes can only occur in the presence of diabatic or frictional processes.

In the numerical modeling experiments described below, changes in EPV are determined following the vortex as defined by the area within a closed contour of potential temperature on the 2 PVU surface. This technique will be used to quantify changes in vortex strength by evaluating (1) within the closed tropopause potential temperature contour. Diabatic tendencies in the numerical model derive from radiation, latent heating, planetary boundary layer processes, convection, and dissipation, which are denoted by $\theta_{t,rad}$, $\theta_{t,lh}$, $\theta_{t,pbl}$, $\theta_{t,cumulus}$, and $\theta_{t,mix}$, respectively. The thermodynamic equation then takes the form

$$\frac{D\theta}{Dt} = \theta_{t,rad} + \theta_{t,lh} + \theta_{t,pbl} + \theta_{t,cumulus} + \theta_{t,mix}. \tag{2}$$

The tendency terms on the right-hand side of the above equation can be used to calculate EPV tendencies due to the first right-hand side term of (1). Similarly, the frictional vector $\vec{F}$ is used to calculate EPV tendencies due to the second right-hand side term of (1) when evaluating error in the diabatic EPV tendencies described subsequently.

An estimate of the error in the diabatic EPV tendencies is made by comparing diabatic and adiabatic residuals, which are defined by:

$$R_d = \left[\frac{\partial \Pi}{\partial t} - \vec{U} \cdot \nabla \Pi\right]_d - \frac{\vec{\omega_a}}{\rho} \cdot \nabla \frac{D\theta}{Dt} - \frac{\nabla \theta}{\rho} \cdot \left(\nabla \times \frac{\vec{F}}{\rho}\right) \tag{3}$$

$$R_a = \left[\frac{\partial \Pi}{\partial t} - \vec{U} \cdot \nabla \Pi\right]_a. \tag{4}$$

The adiabatic residual, R_a, is derived by an integration of the model without diabatic processes. Note that some sources of error, such as implicit model diffusion (due to the time integration scheme), and grid interpolation, are difficult to estimate and are not explicitly considered here. Since estimates of the time derivatives and advection are leading sources of error common to

both R_a and R_d, we define the diabatic residual as the difference between (3) and (4), which isolates an estimate of the part of the error due only to the diabatic tendencies.

Clouds can play an important role in how radiation is redistributed in the atmosphere (e.g. Turner 2005), which in turn affects how potential vorticity is redistributed (See equation 1). In anticipation of the PV budget analysis in the following section, a cartoon is provided here to illustrate the primary patterns. Since the Arctic is characterized by low temperature and high cloud cover (e.g. Curry et al. 1996), we expect that near the tropopause, the dominant diabatic contributions are from radiation and latent heating. Considering this expectaction and only the vertical component of vorticity, then using (2), (1) simplifies to $\frac{D\Pi}{Dt} \simeq \zeta_a \frac{\partial}{\partial z} \left(\theta_{t,rad} + \theta_{t,lh}\right)$ and the vertical structure of the EPV tendencies are due to vertical gradients of latent heating and radiation. Fig. 2 shows a cartoon of the expected cloud–radiative feedback processes that affect PV. If latent heating is relatively small compared to cloud-top radiational cooling, a positive EPV tendency is expected just above the cloud top. Conversely, when latent heating is relatively large with respect to radiation, a negative EPV tendency is expected near the cloud top. We hypothesize that in the Arctic, vortex intensification occurs when radiative tendencies dominate latent heating tendencies which, by the Clausius-Clapeyron equation, is more likely at colder temperatures typical of the Arctic.

4. Case study

The cyclonic TPV under consideration occurred during the 37 day period from 1 November to 7 December 2005, and is identified following the local minimum in tropopause potential temperature derived from the Global Forecast System (GFS) analyses (Fig. 3a); for clarity, only

the first 25 days of the vortex track are shown. The vortex originates over Siberia and travels slowly, nearly in a loop, arriving on the northern Siberia coast near the Taymyr peninsula after one week. The vortex continues to move slowly northward for another week, at an average speed of 5–10 ms^{-1}, remaining near the central Arctic Ocean. It reaches the northwestern Canadian Archipelago on day 18 of its life-cycle, thereafter accelerating, turning southeast, and reaching Hudson Bay by day 21. The vortex performs a loop pattern between the Great Lakes and Hudson Bay, and by day 37 can no longer be tracked by the presence of closed tropopause potential temperature contours near the northeastern United States Atlantic coast.

The corresponding time series of vortex core potential temperature from 1 November (Day 0) to 26 November 2005 (Day 25) is shown in Fig. 3b. Tropopause potential temperature steadily decreases for about 17 days, reflecting an intensifying cyclone. The strengthening trend continues from day 17 until day 22, however, there are large fluctuations during this time period, perhaps due to the low tropopause interacting with an Arctic low-level temperature inversion, a commonly observed feature in this region (e.g. Curry 1983). Tropopause potential temperature values of around 260 K and tropopause pressure values near 800 hPa reflect an intense vortex at this time. A transition from a strengthening trend to a weakening trend begins around day 22. During this time, the cyclone moves southward over Hudson Bay, and a significant surface low pressure center forms.

A sequence of radiosonde profiles at Coral Harbour, Nunavut, Canada and the corresponding GFS tropopause analyses capture the vortex vertical structure near Hudson Bay (Fig. 4). Before the cyclone reaches Coral Harbour, the observed tropopause pressure is approximately 350 hPa with westerly winds reflecting a cyclonic circulation located north of the station (Fig. 4a,b). At 00 UTC 22 November 2005, the cyclone is closest to the Coral Harbour radiosonde station, with

a tropopause pressure of 650 hPa, compared to 675 hPa in the GFS analysis (Fig. 4c,d). The maximum tropopause pressure of 807 hPa is located north of the station in the GFS analysis (Fig. 4d). As the vortex moves southward over Hudson Bay, the tropopause pressure at Coral Harbour slowly rises (Fig. 4e-h) and a surface low pressure system intensifies over Hudson Bay. The surface low pressure system appears similar to a case examined by Albright et al. (1995), who found that its formation was a result of convective latent heat release when an upper-level cold-core low pressure system moved over a relatively warm, ice-free segment of Hudson Bay, enhancing surface heat and moisture fluxes. In the present case, a complex surface low pressure structure is evident in a Moderate Resolution Imaging Spectroradiometer (MODIS; Fig. 5) with a cyclonic arc of clouds found over southwestern Hudson Bay.

5. Numerical simulation and PV budget

Numerical simulations are performed for two stages in the life cycle of the case just described. The first simulation examines the intensification phase, and the second simulation examines the weakening phase over Hudson Bay. We note that although the vortex core potential temperature exhibits an increase (weakening) during second phase (Fig. 3), area averages shown subsequently over the entire vortex reveal little change; nevertheless, we shall refer to this time as the weakening phase. These simulations are used to estimate the diabatic terms in the PV budget as described in Section 3.

a. Numerical Model

We use the Advanced Research Weather (ARW) version of the Weather Research and Forecasting (WRF) model version 2.1.2 and the WRF Standard Initialization (WRF-SI) Version

2.1 (Skamarock et al. 2005). Time integration is achieved by a 3rd-order accurate Runge-Kutta method, and horizontal advection by a 5th-order accurate scheme. A horizontal grid spacing of $\Delta x = \Delta y = 30$ km is used, with 31 vertical levels and a model time step of $\Delta t = 120$ seconds. The vertical coordinate system is a terrain-following coordinate defined by $\eta = p_h/p_{hs}$ where p_h is the hydrostatic pressure and p_{hs} is the hydrostatic surface pressure. The following physics schemes are used: Rapid Radiative Transfer Model (RRTM) longwave radiation, NASA Goddard shortwave radiation, WSM 5-class microphysics, Kain-Fritsch cumulus convection, YSU planetary boundary layer, thermal diffusion surface physics, and Monin-Obukhov surface layer physics.

The strengthening and weakening phases that are simulated here occur while the vortex is over Siberia and near Hudson Bay, respectively, and will be referred to as the Siberia and Hudson Bay segments. Forecasts are initialized using Global Forecasting System (GFS) analyses on 5 November 2005 for the Siberia segment and on 22 November 2005 for the Hudson Bay segment, with boundary conditions derived from six-hourly GFS analyses and intervening 3 hour forecasts.

b. PV budget of intensification phase

In terms of vortex tropopause core potential temperature, both the WRF forecast and GFS analysis show a deepening cyclonic vortex for the Siberia segment (Fig. 6a). Time-height sections of EPV tendencies due to all diabatic PV components are shown in Fig. 7 for the days corresponding to those in Fig. 6a. All fields are averaged spatially for tropopause potential temperature below 285 K, which represents the last closed contour in the field. The net diabatic effect is the creation of positive EPV near the tropopause, which indicates that the tropopause

is lowering in time (Fig. 7a). Cloud water (sum of liquid and ice mixing ratios) reveals that clouds extend throughout the troposphere, and EPV generation from the radiational diabatic component is concentrated near the top of the clouds, primarily near the tropopause (Fig. 7b). Latent heating contributes to EPV destruction in the upper troposphere and to some extent near the tropopause; however, the most negative EPV tendencies are found below the tropopause (Fig. 7c). The results show that the tendency to create EPV from cloud-top radiational cooling dominates the tendency to destroy EPV from latent heating (Fig. 7d).

Fig. 9a shows profiles of the EPV components averaged over the time period corresponding to the time-height sections of Fig. 7 (5–10 November 2005). The largest EPV tendency near the tropopause comes from advection, followed by the full diabatic term (Fig. 9a). Decomposing the full diabatic term shows that the most significant diabatic component near the tropopause is due to radiation, which accounts for nearly all of the total diabatic term (Fig. 9b). EPV destruction due to latent heating peaks 75 hPa below the tropopause, whereas creation of radiational EPV peaks closer to the tropopause, which is qualitatively consistent with the conceptual picture given in Fig. 2a, where radiational effects were assumed to dominate latent heating effects.

c. PV budget of weakening phase

The WRF forecast and GFS analysis both show vortex core tropopause potential temperature increasing, which indicates a weakening cyclonic vortex during the Hudson Bay simulation (Fig. 6b). In this simulation, all fields are averaged spatially for tropopause potential temperature below 280 K, representing the last closed contour during this segment. Time-height sections do not show significant contributions to EPV tendency from diabatic effects

near the tropopause (Fig. 8a). The tropopause height remains relatively unchanged near 600 hPa, and although cloud mass extends throughout the troposphere, the main concentration is in the lower troposphere near 850 hPa (Fig. 8b). Moreover, cloud mixing ratios are higher in this segment compared to the Siberia segment, and the clouds are also composed mainly of supercooled liquid drops, rather than ice crystals as in the Siberia segment (not shown). Radiation contributes to weak positive EPV tendencies in the upper troposphere (Fig. 8b). A dipole of EPV tendency straddles the maximum in cloud mass near 850 hPa, with weak negative tendencies in the upper troposphere (Fig. 8c). Diabatic tendencies from the remaining terms (planetary boundary layer processes, convection, and dissipation) are complicated, but affect PV mainly in the lower troposphere (Fig. 8d).

Time-mean vertical profiles of EPV tendency components for this segment (averaged over the times shown in Fig. 8) indicate that the advection and time tendency terms dominate the budget near the tropopause, and that the diabatic component is comparatively small (Fig. 9c). Profiles of the individual diabatic terms are more complex during this time period compared to the Siberia segment, with most diabatic components making comparably sized contributions near the tropopause (Fig. 9d). Moreover, the effective residual term is of comparable magnitude to the full diabatic term as well as individual diabatic components, suggesting that the results are less conclusive than for the Siberia segment.

6. Summary and concluding remarks

Diabatic mechanisms that affect the intensity of a cyclonic tropopause polar vortex (TPV) have been quantified in a potential vorticity framework. Motivation for the case study derived

from an Arctic vortex census, which showed that the maximum occurrence of tropopause cyclogenesis, cyclolysis, growth, and decay are found near Baffin Island, Canada. Moreover, the fact that no significant relationship was found between large-scale circulation patterns and vortex intensity suggests that local processes are most important. A long-lived case was selected for closer examination, including a review of observational evidence for the event and a potential vorticity diagnosis of the strengthening and weakening phases of the vortex life cycle.

Given that latent heating typically peaks well below the tropopause, reducing potential vorticity near the tropopause, we hypothesized that cloud-top radiational cooling is important for increasing potential vorticity near the tropopause. Results from the case study provide supporting evidence for this hypothesis during the time of observed intensification. Later in the life cycle of the event, when the vortex is located over the unfrozen water of Hudson Bay, latent heating increases, primarily in the lower troposphere. The small loss in potential vorticity near the tropopause is nearly offset by a small positive tendency from the radiational tendency, resulting in little change in tropopause position averaged over the vortex area, consistent with the observed tendency.

It remains for future work to determine the generality of the results determined for the case study presented here. The results suggest that cyclonic tropopause vortex intensification is favored for low temperatures, since latent heating decreases approximately exponentially with temperature. This implies that the population characteristics of these ubiquitous, persistent features of the Arctic may change during the projected warmer Arctic climate. This possibility suggests another fertile area for research.

Acknowledgments.

This paper is based in part on the first author's Masters thesis. This research was sponsored by the National Science Foundation through awards ATM-0228804 and ATM-0552004 made to the University of Washington.

References

Albright, M. D., R. J. Reed, and D. W. Ovens, 1995: Origin and structure of a numerically simulated polar low over hudson bay. *Tellus*, **47A**, 834–848.

Curry, J. A., 1983: On the formation of continental polar air. *J. Atmos. Sci.*, **40 (9)**, 2278–2292.

Curry, J. A., W. B. Rossow, D. Randall, and J. L. Schramm, 1996: Overview of arctic cloud and radiation characteristics. *J. Climate*, **9**, 1731–1764.

Davis, C. A. and K. A. Emanuel, 1991: Potential vorticity diagnostics of cyclogenesis. *Mon. Wea. Rev.*, **119 (8)**, 1929–1953.

Hakim, G. J. and A. K. Canavan, 2005: Observed cyclone-anticyclone tropopause asymmetries. *J. Atmos. Sci.*, **62 (1)**, 231–240.

Hoskins, B. J., M. E. McIntyre, and A. W. Robertson, 1985: On the use and significance of isentropic potential vorticity maps. *Quart. J. Roy. Meteor. Soc.*, **111 (470)**, 877–946.

Kalnay, E. and collaborators, 1996: The NCEP/NCAR 40-year reanalysis project. *Bull. Amer. Meteor. Soc.*, **77**, 437–472.

Nolan, D. S. and L. D. Grasso, 2003: Nonhydrostatic, three-dimensional perturbations to balanced, hurricane-like vortices. part ii: Symmetric response and nonlinear simulations. *J. Atmos. Sci.*, **60 (22)**, 2717–2745.

Pedlosky, J., 1998: *Geophysical Fluid Dynamics*, Vol. 84. 2d ed., Springer, 728 pp.

Schubert, W. H. and J. J. Hack, 1983: Transformed eliassen balanced vortex model. *J. Atmos. Sci.*, **40**, 1571–1583.

Shapiro, L. J. and H. E. Willoughby, 1982: The response of balanced hurricanes to local sources of heat and momentum. *J. Atmos. Sci.*, **39 (2)**, 378–394.

Skamarock, W. B., J. B. Klemp, J. Dudhia, D. O. Gill, D. M. Barker, W. Wang, and J. G. Powers, 2005: A description of the advanced research wrf version 2. Tech. rep., NCAR.

Stoelinga, M. T., 1996: A potential vorticity-based study of the role of diabatic heating and friction in a numerically simulated baroclinic cyclone. *Mon. Wea. Rev.*, **124 (5)**, 849–874.

Turner, D. D., 2005: Arctic mixed-phase cloud properties from aeri lidar observations: Algorithm and results from sheba. *J. Appl. Meteor.*, **44**, 427–444.

Wirth, V., 1995: Diabatic heating in an axisymmetric cut-off cyclone and related stratosphere-troposphere exchange. *Quart. J. Roy. Meteor. Soc.*, **121 (521)**, 127–147.

Zierl, B. and V. Wirth, 1997: The influence of radiation on tropopause behaviour and stratosphere-troposphere exchange in an upper tropospheric anticyclone. *J. Geophys. Res.*, **102 (23)**, 883–894.

List of Figures

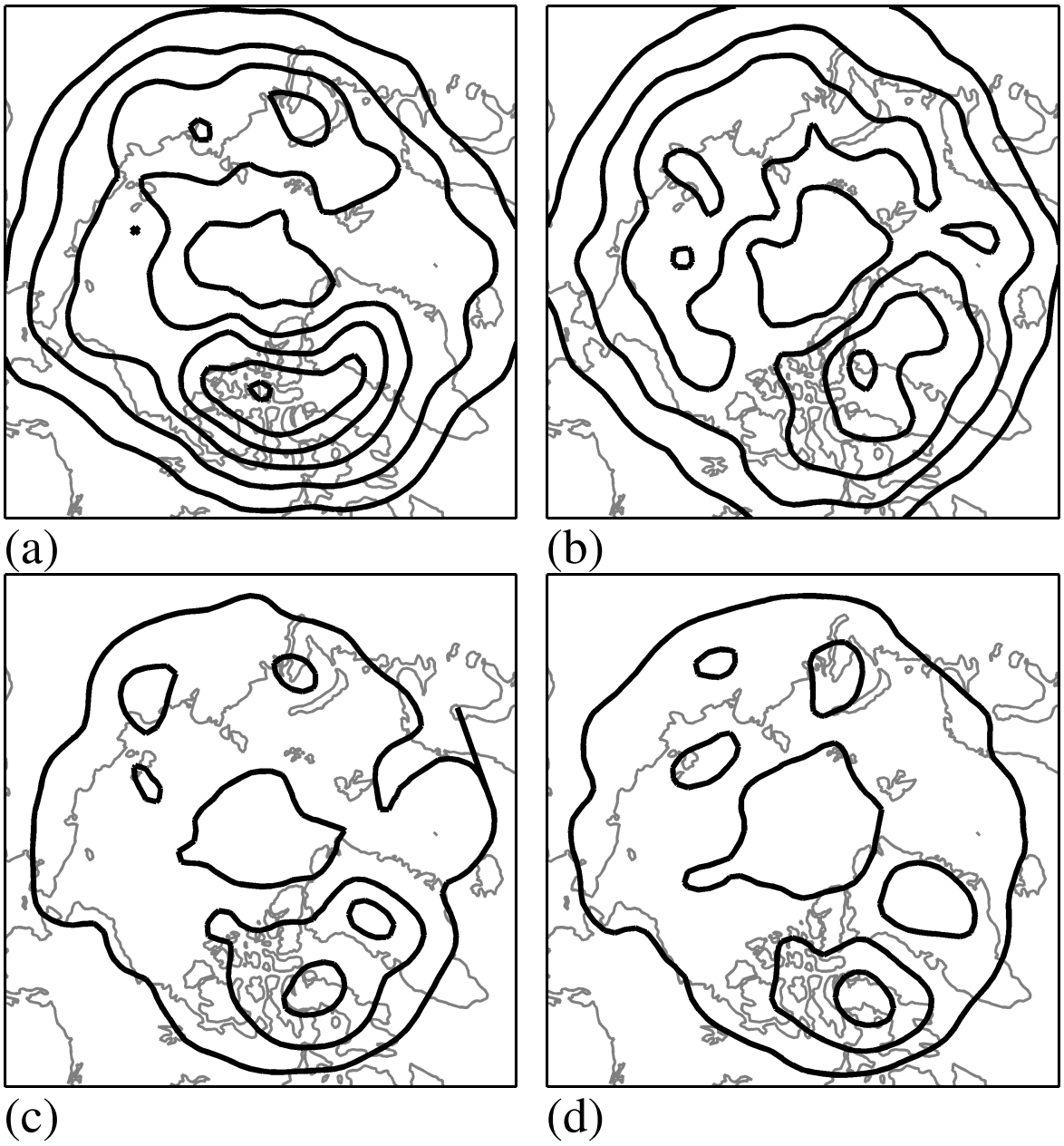

FIG. 1. Area-weighted occurrence of tropopause polar (a) cyclogenesis, (b) cyclolysis, (c) cyclone growth, and (d) cyclone decay. Values are equal to the number of events within a 5° latitude × 15° longitude box divided by the cosine of latitude with a contour interval of 100. Only vortices lasting at least two days and which spent at least 60% of their lifetimes north of 65°N latitude are considered.

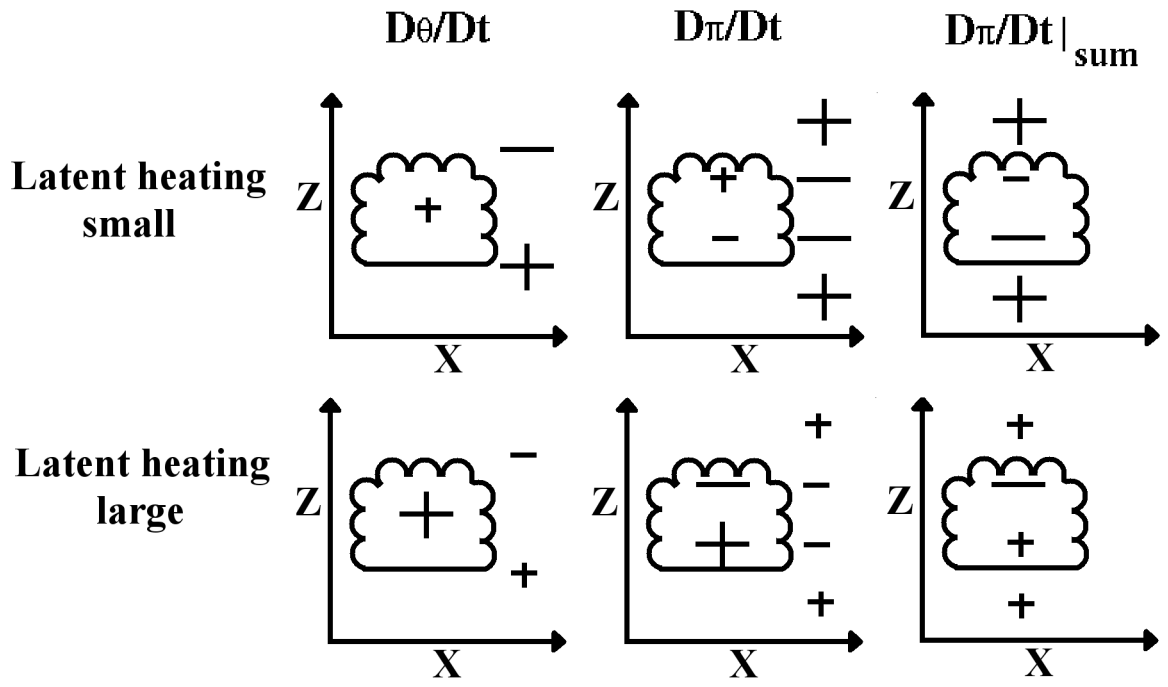

FIG. 2. Cartoon illustrating the relative importance of latent and radiational heating on potential vorticity near clouds. The top row represents the case when latent heating is relatively small compared to radiational heating and the bottom row represents the case where latent heating is relatively large compared to radiational heating. "+" symbols represent positive values and "-" symbols represent negative values, and magnitudes are denoted by relative size of the symbols. Left panels show the total heating ($\frac{D\theta}{Dt}$), where symbols inside the cloud represent latent heating and outside the cloud represent radiational heating. The middle panel represents the independent EPV tendencies ($\frac{D\pi}{Dt}$), where symbols inside the cloud represent EPV tendencies from latent heating and outside the cloud represent EPV tendencies from radiation. The right panel represents net EPV tendencies ($\frac{D\pi}{Dt}\ |_{sum}$) resulting from the combined effects of latent and radiational heating.

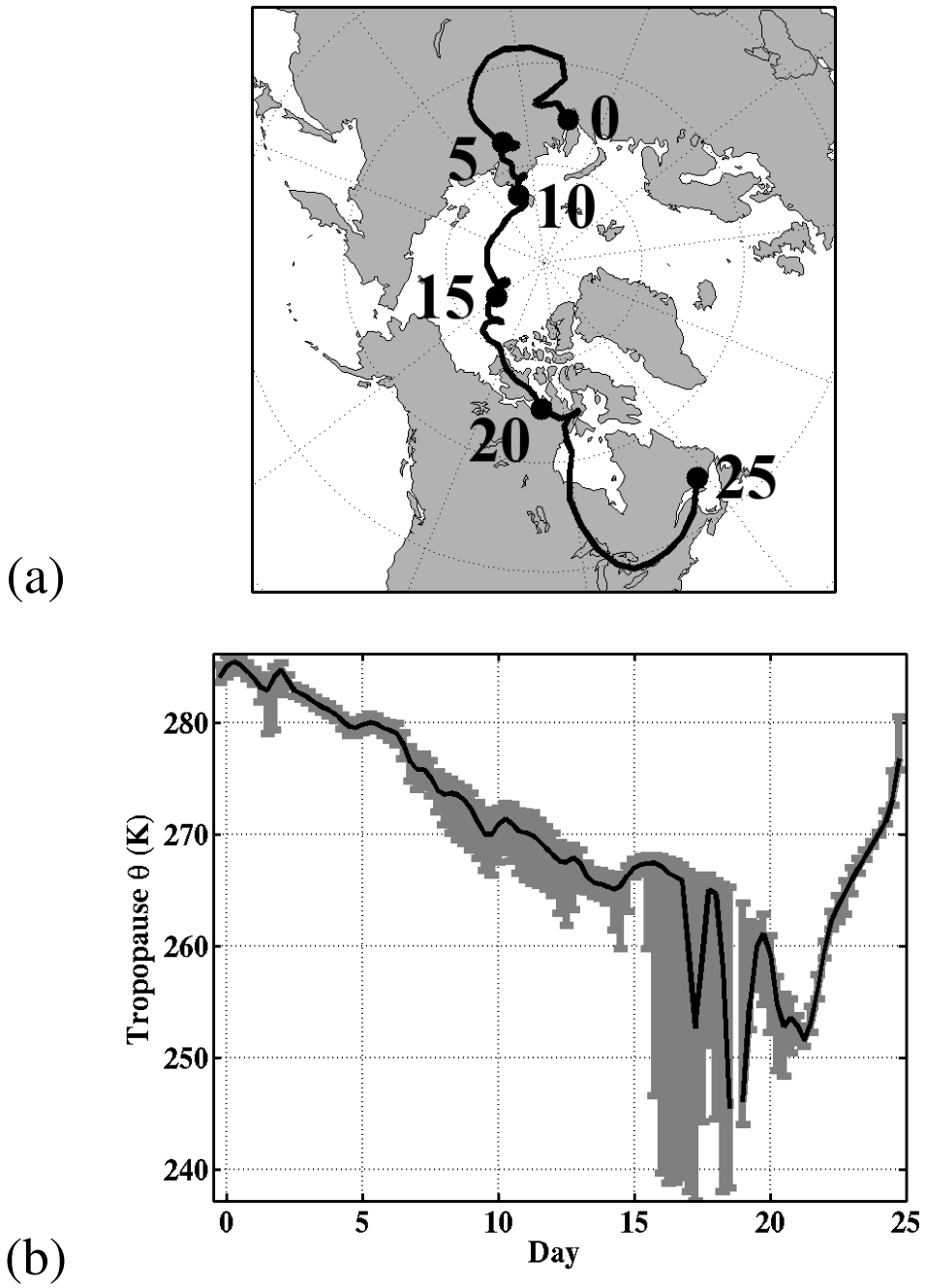

FIG. 3. GFS tropopause analysis of the TPV cyclone during 1–26 November 2005. (a) Vortex track following the minimum potential temperature on the 2 PVU surface and (b) corresponding time series of tropopause minimum potential temperature with the shaded areas representing a range of tropopause definitions from 1.75–2.25 PVU; this range provides a measure of sensitivity to the tropopause definition. Solid circles in (a) denote days since the beginning of the vortex track, which also correspond to the abssica in (b). A $1-2-1$ smoother is applied to the time series and values below 245 K are suppressed.

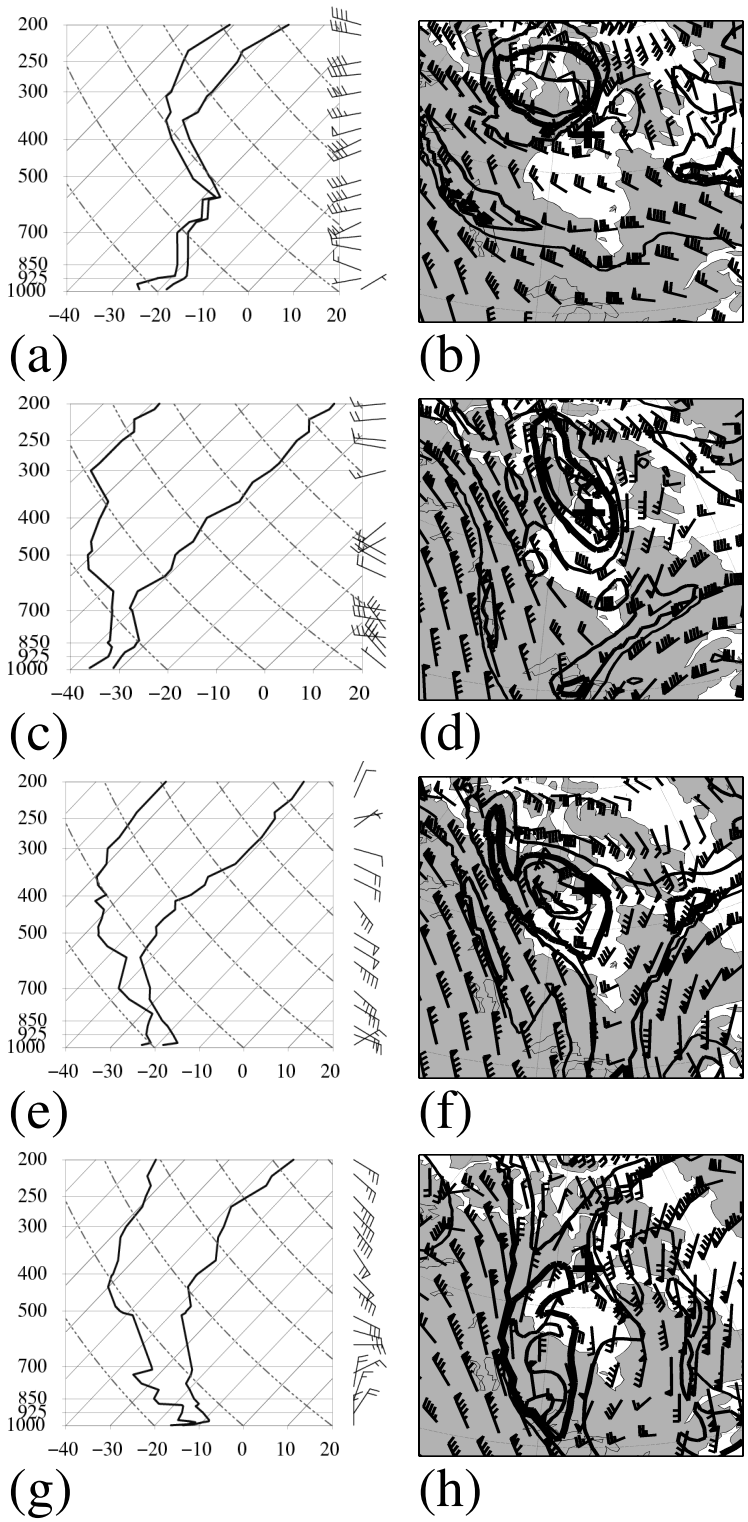

FIG. 4. SKEWT–log p diagram of radiosonde profiles of temperature (° C) and dew point temperature (° C) at Coral Harbour, Nunavut Canada (left panels) and GFS tropopause pressure (contours every 100 hPa with the 500 hPa contour shown bold for reference) and tropopause wind (knots) (right panel) at 00 UTC on (a) and (b) 21 November 2005, (c) and (d) 22 November 2005, (e) and (f) 23 November 2005, and (g) and (h) 24 November 2005. Coral Harbour is located on the north side of Hudson Bay near the bold '+' symbol.

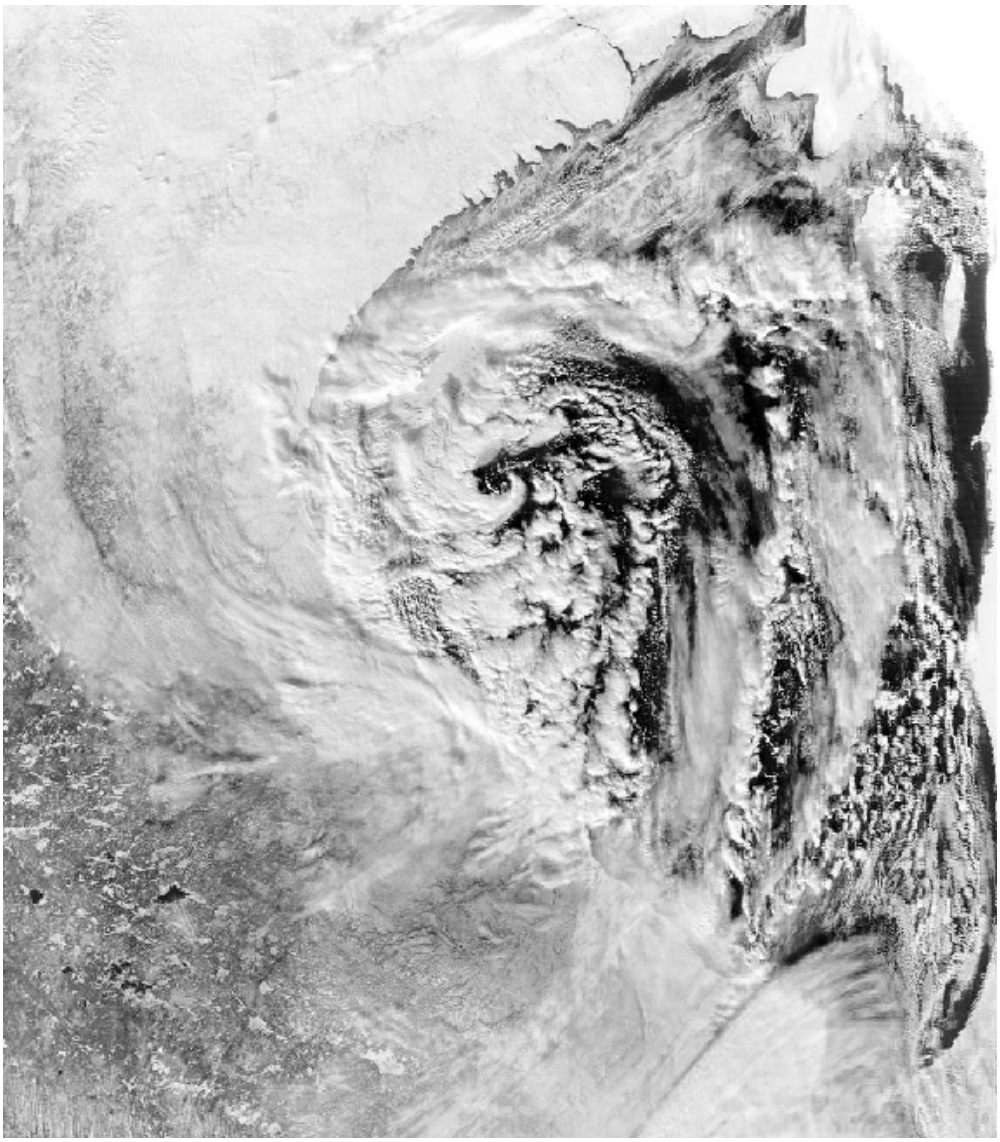

FIG. 5. Moderate Resolution Imaging Spectroradiometer (MODIS) visible satellite image from 1845 UTC 23 November 2005. Field of view is the western side of Hudson Bay.

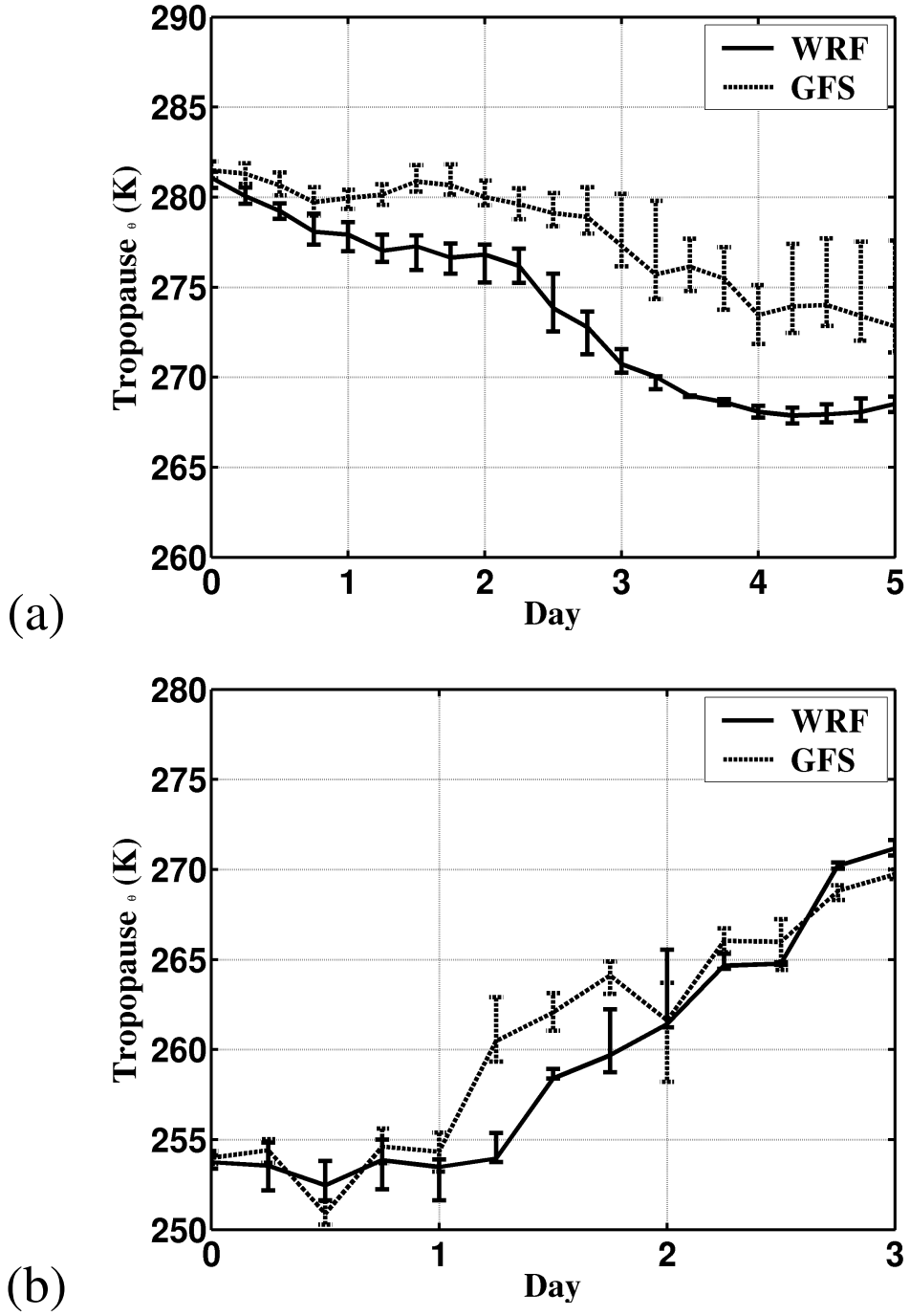

FIG. 6. Tropopause potential temperature (K) at the vortex core from GFS analyses (dashed lines) and WRF simulations (solid lines) initialized (a) 00 UTC 5 November 2005 C over Siberia, Russia and (b) 00 UTC 22 November 2005 over Hudson Bay, Canada. Vertical bars represent values derived from tropopause definitions ranging from 2.25 PVU to 1.75 PVU.

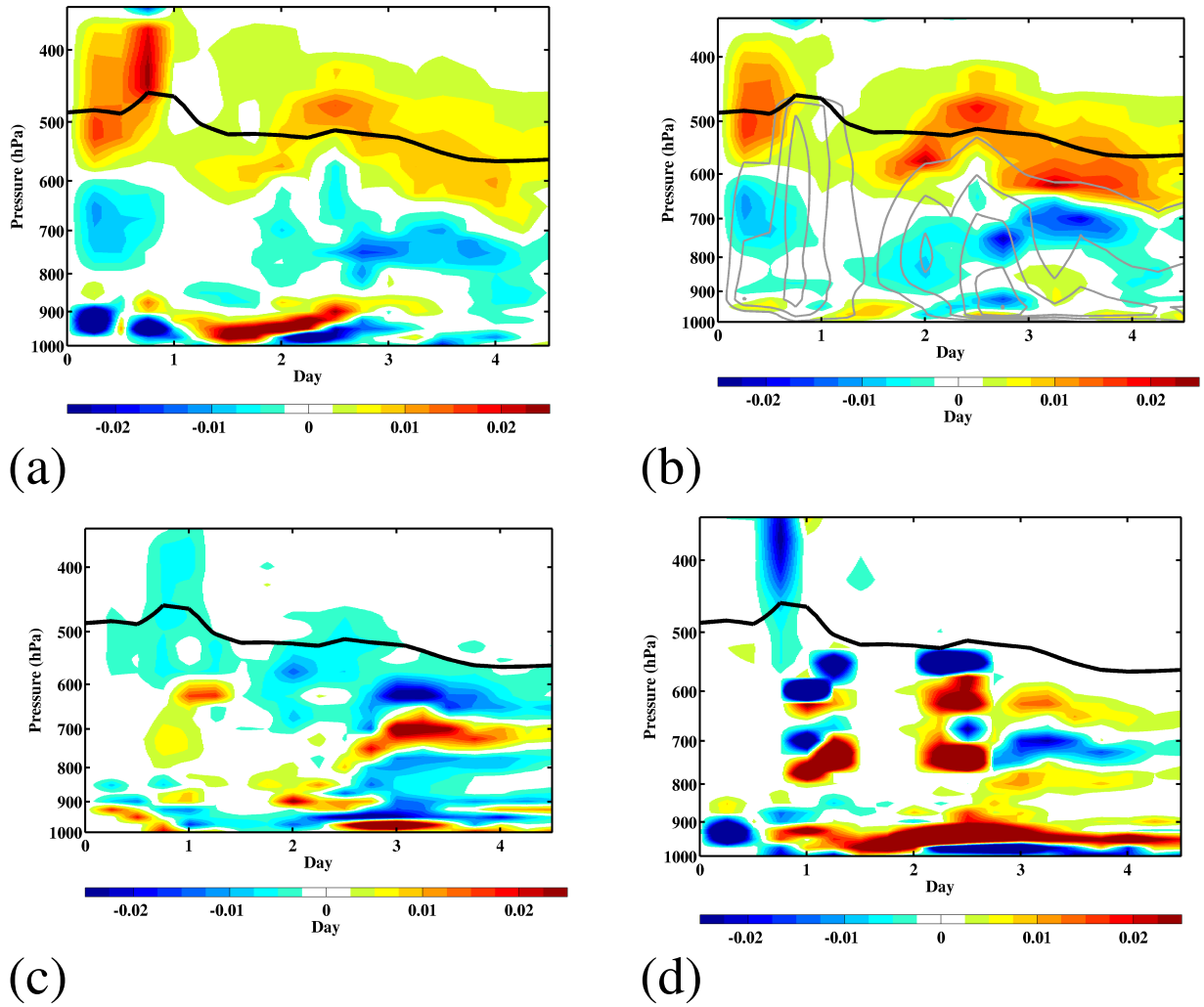

FIG. 7. Time–height sections from a WRF simulation during 00 UTC 5 November 2005 to 00 UTC 10 November of EPV tendencies (PVU hour^{-1}) due to (a) all diabatic processes, (b) radiation (colors) and cloud water (sum of liquid and ice mixing ratios; contours every 0.004 g kg^{-1}), (c) latent heating, and (d) the sum of the planetary boundary layer scheme, cumulus scheme, and frictional processes. All fields are averaged within the area encompassed by the 285 K closed tropopause potential temperature contour. The bold black line represents the 2 PVU surface. Labels on the abscissa are days from the start of the simulation. EPV tendency ccolor interval is 0.0025 PVU hour^{-1}.

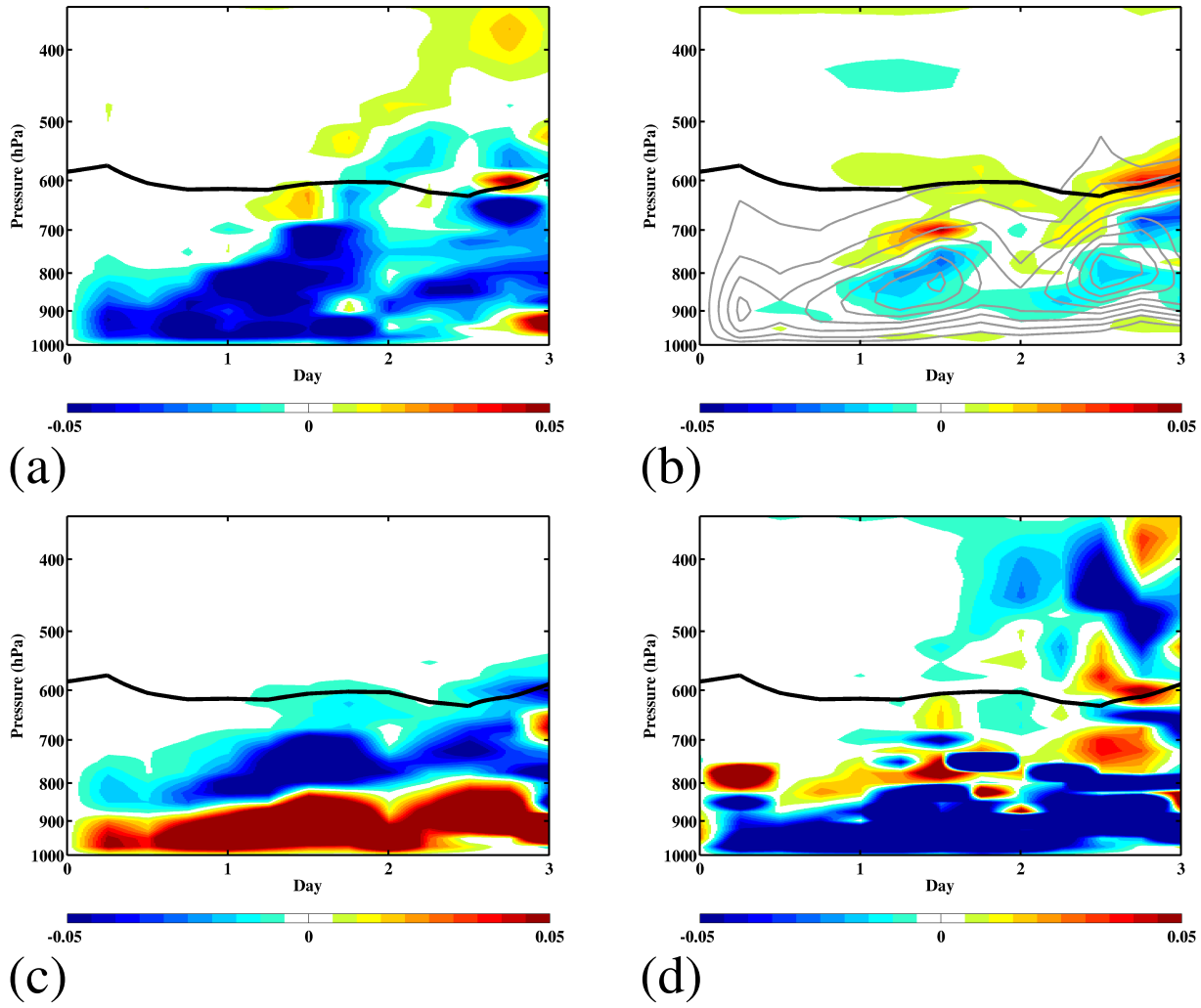

FIG. 8. As in Figure 7, except for the Hudson Bay simulation during 00 UTC 22 November 2005 to 12 UTC 24 November with averages within the 280 K tropopause potential temperature closed contour.

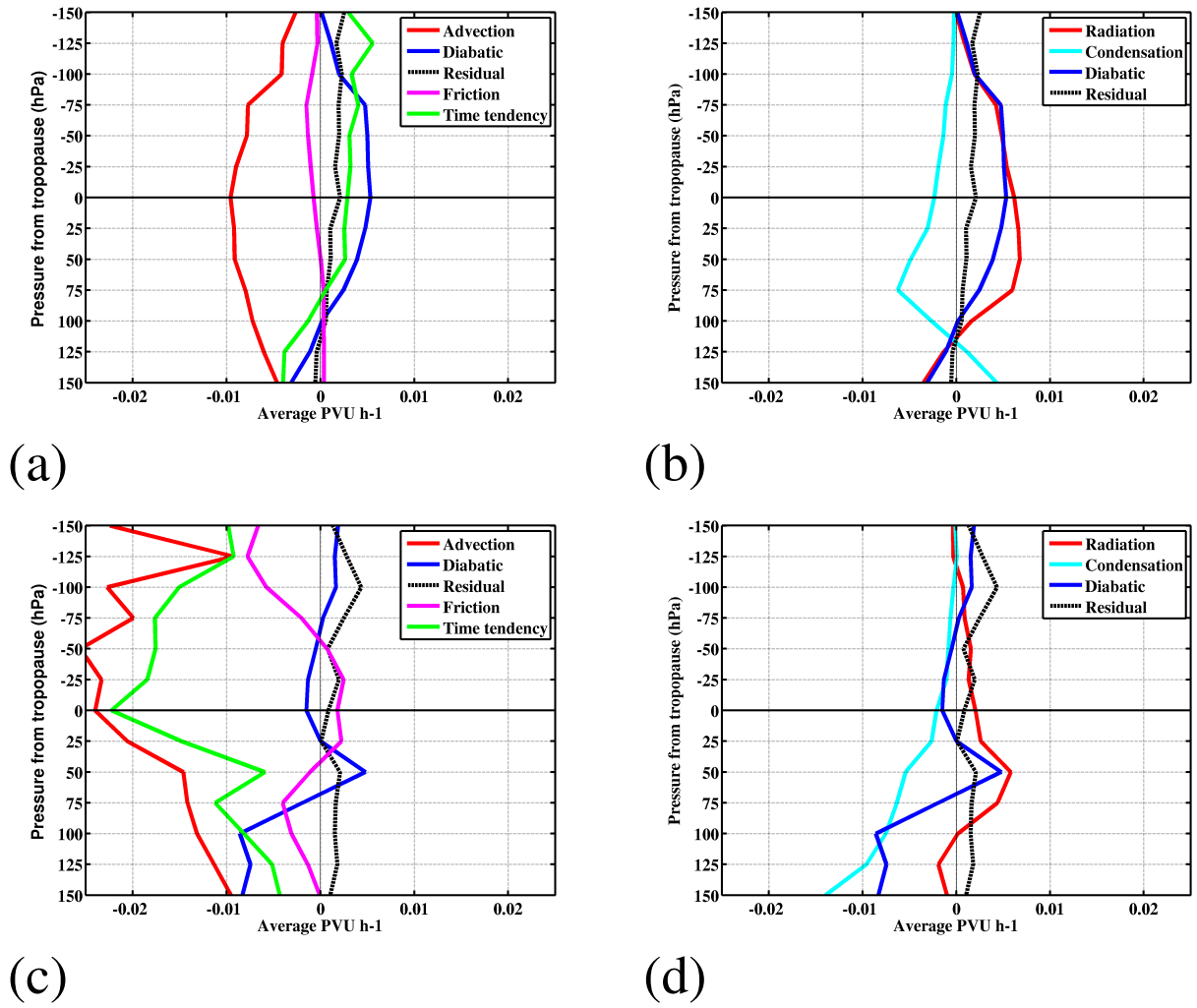

FIG. 9. Time mean vertical profiles of EPV tendency (PVU hour^{-1}) from all components (left) and diabatic contributions (right) for the (a),(b) Siberia simulation and (c),(d) Hudson Bay simulation. Vertical levels are pressure coordinates (hPa) relative to the tropopause; zero denotes the tropopause. All values are averaged within the 285 K closed tropopause potential temperature contour for the Siberia simulations and 280 K for the Hudson Bay simulation.